Chirality Nano-Sensor with Direct Electric Readout by Coupling of Nanofloret Localized Plasmons with Electronic Transport

Amir Ziv[a], Omer Shoseyov[a], Prajith Karadan[b], Brian P. Bloom[c], Sharone Goldring[a], Tzuriel S. Metzger[a], Shira Yochelis[a], David H. Waldeck[c], Roie Yerushalmi[b*], and Yossi Paltiel[a*]

a) Department of Applied Physics, The Hebrew University, Jerusalem, 9190401

b) Institute of Chemistry, The Hebrew University, Jerusalem, 9290401.

c) Chemistry Department, University of Pittsburgh, Pittsburgh, Pennsylvania 15260, United States

ABSTRACT: The detection of enantiopurity for small sample quantities is crucial, particularly in the pharmaceutical industry; however, existing methodologies rely on specific chiral recognition elements, or complex optical systems limiting its utility. A nanoscale chirality sensor, for continuously monitoring molecular chirality using an electric circuit readout, is presented. This device design represents an alternative real-time scalable approach for chiral recognition of small quantity samples (less than 10^3 adsorbed molecules). The active device component relies on a gold nanofloret hybrid structure, i.e., a high aspect ratio semiconductor-metal hybrid nanosystem in which a SiGe nanowire tip is selectively decorated with gold metallic cap. The tip mechanically touches a counter electrode to generate a nanojunction, and, upon exposure to molecules, a metal-molecule-metal junction is formed. Adsorption of chiral molecules at the gold tip induces chirality in the localized plasmonic resonance at the electrode-tip junction and manifests in an enantiospecific current response.

Keywords: chirality sensing, nanosensor, nanowires, localized plasmon, plasmon-molecular coupling

Many of the biomolecular building blocks of living organisms possess a specific chirality; e.g. sugars are dextrorotatory and proteins and amino acids are levorotatory.[1] The ubiquitous nature of chirality in biological processes often necessitates enantiomeric specificity for desired functionality and preventing adverse effects.[2] As such, the determination of chiral purity is of paramount importance for drug development,[3] as well as in the food[4] and agriculture industry,[5] and even in astrobiology.[6] State of the art methods for probing enantiopurity can typically be divided into four main categories: chiroptical methods, which involve the direct interaction of light with the substance to be characterized,[7] chiral chromatography, NMR of a mixture of enantiomers upon reaction with a chiral derivatizing agent, and device-based sensors.

Chiroptical methods, such as electronic circular dichroism (ECD),[8] is based on the different excitation of an electron from a molecular ground state to an excited state under left and right circularly polarized electromagnetic radiation (LCP and RCP respectively). The ECD signal can be related to the structure of the molecule.[9,10] Vibrational circular dichroism (VCD),[11] and optical rotary dispersion[12] are also commonly employed for determining enantiomeric excess; however the measurement typically requires large and complex optical setups.[13–15] By employing a chiral reagent to create diastereomeric adducts the enantiomeric difference can be detected by analyzing for the different diastereomers. This principle can be employed in both NMR[16] and high performance liquid chromatography[17] (HPLC). Alternatively, chiral chromatography can separate enantiomers through enantioselective interactions of the analyte with a chiral stationary phase; typically cyclodextrin is employed because it is cheap and binds to a large variety of molecules. Despite the general applicability of chromatography, the experimental history of the column can cause memory effects which impact resolution [J. Chromatogr. A, 2002, 945, 139-146. J. Chromatogr. A, 2011, 1218, 6302-6307.] and thus require experiments to assess and condition

the column. Chiral sensing with a device often requires a chiral recognition element which functions as a mediator between the chiral analyte and the device. As such, the specificity of the sensor must be tailored to each individual analyte of interest. Examples for device based sensors include electrochemical sensors,[18,19] gravimetric-mass sensors,[20] field-effect,[21,22] chemiresistors,[23] chemocapacitors,[24] and surface plasmon based sensors.[25–27] It is highly desirable to combine the favorable attributes of chiroptical based methods, universally applicable to all analytes, with the compactness and real-time based response of a sensor device. In this study, a chirality sensor is fabricated in which the adsorption of a chiral molecule induces a change in the localized surface plasmon response of a gold nanofloret (Au-NF) and creates an electrical response through a nanojunction.[28]

Localized surface plasmon resonance (LSPR) arises from the coherent oscillation of conduction electrons in a metallic nanoparticle with dimensions smaller than the illumination wavelength. The LSPR is characterized by an enhancement of the electromagnetic field and confinement to the nanoparticle dimensions. Previous studies have shown that coating a metallic nanoparticle with chiral molecules enhances the electronic circular dichroism signal, and it induces chirality on the LSPR mode.[29–32] This work shows that the integration of a chiral plasmonic metastructure with an electrode can be used to generate a chiroptical response that can be translated directly into an electrical signal readout.[33]

The device reported herein utilizes the change in LSPR, upon adsorption of chiral analytes, to generate an enantiospecific current response. The device is fabricated by suspending a self-formed hybrid Au-NF, consisting of a gold nanocap at the tip of a high aspect ratio semiconducting SiGe nanowire (NW), between two metallic contacts. The Au-NF synthesis and device fabrication combines bottom-up synthesis and standard photolithography methods, which have been described

in detail elsewhere.[28,34,35] The detection scheme is illustrated in Figure 1a, and the inset shows an SEM image of the Au-NF consisting of the SiGe NW and a metallic Au tip in contact with a macroscopic Ti metal pad. Upon illumination, the LSPR of the gold nanocap which is coupled to the SiGe NW modulates the current flow through the nanojunction. Previous studies[36] have compared experimental and simulation results to show that the LSPR mode arises from the unique metastructure of the gold cap, comprising a cluster of gold nanoparticles separated by a GeOx dielectric layer. A tunneling barrier exists between the gold cap and the SiGe semiconductor, and the excitation of the LSPR on the Au modulates the current flow through the barrier. The device sensitivity is determined by the LSPR and is spectrally broad, extending to the short-wave infrared spectral region, as we previously reported.[36]

The sensitivity to chiral molecules manifests when the molecules are introduced to the system and they adsorb on the Au tip near the mechanical junction.[34] The adsorbed molecules imprint chirality onto the LSPR of the Au nanocap;[37] and because the LSPR response is coupled to the current through the tunneling barrier[36] an enantiospecific current response manifests. The cap surface area is on the order of 10^{-9} cm^2. By assuming a maximum density of 10^{12} molecules/cm^2 adsorbed on gold, it is estimated that less than 10^3 molecules are adsorbed for a full coverage monolayer formed on the gold cap in each Au-NF junction. The chiral molecules are linked to the gold tip via thiol linkers. The angle of adsorption could differ between molecules in an inhomogeneous manner, however their chirality is the same for all angles and the gold is grained, thus, we expect that the chiral imprinting effect is similar and does not depend too strongly on the adsorption angle.

Figure 1b shows the experimental scheme used for sensing. A voltage bias is applied across the suspended Au-NF and the electrical current through the device is measured, while circularly

polarized laser illumination is focused on the sample with a microscope objective. A CCD camera is used to align the Au-NF junction under the focused spot. Circular polarization is achieved by using a quarter waveplate and alternation between LCP and RCP is achieved by rotating a half waveplate on a motorized stage. Special care was taken to ensure a high degree of circular polarization (see section 6 in the SI for further details) because the high aspect ratio NWs are susceptible to orientation effects from linearly polarized light[38] and deviations in circular polarization may bias the device response. Note that the confinement and enhancement of the electromagnetic field is achieved because of the LSPR at the NF gold nanocap and is not associated with focusing by the objective lens. An objective lens with a relatively low numerical aperture (0.4 NA) was selected since using higher NA lens may result in changes of the light polarization state.[39,40] A constant voltage of 1V was applied and the current was measured as a function of time with a time resolution of 50 ms, while alternating between RCP and LCP polarizations for periods of 30 seconds.

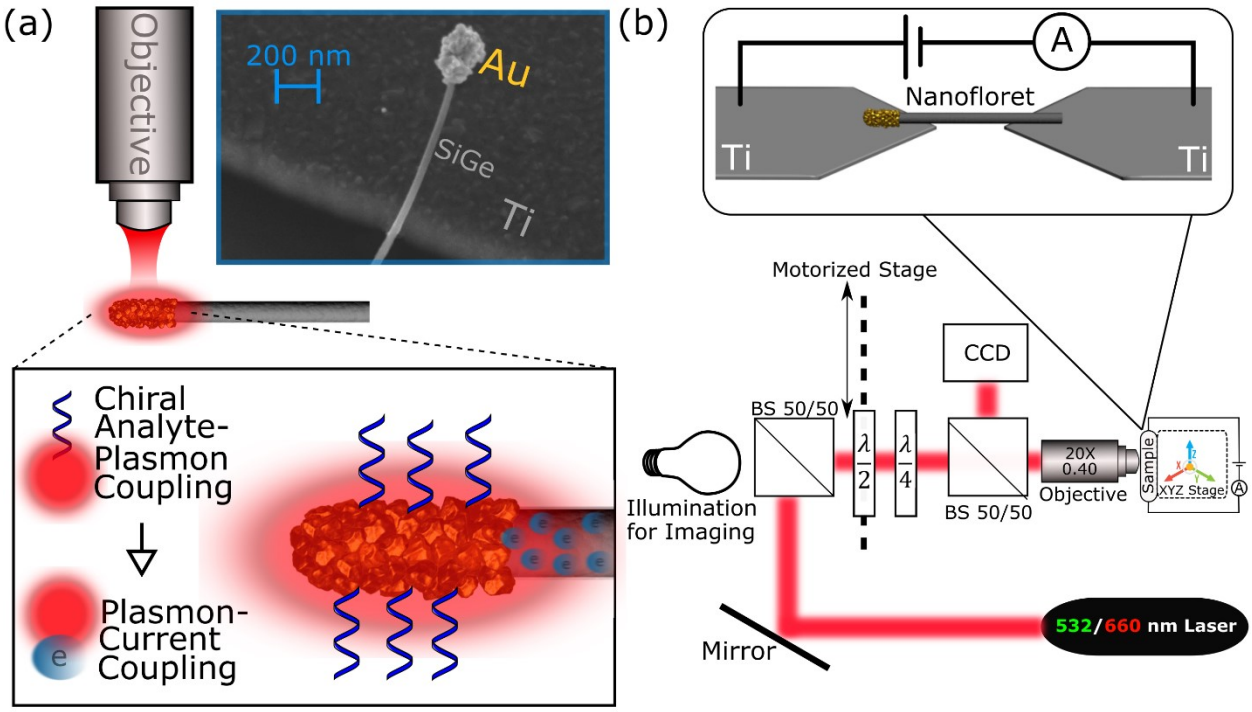

Figure 1. *Illustration of the device measurement scheme a) Au-NF junction is illuminated with focused continuous wave laser radiation. The chiral substance is coupled to the localized surface plasmon, which is in turn coupled to the current that passes through the Au-NF. Inset: SEM image of the Au-NF device, a semiconducting (SiGe) nanowire with a gold nanocap at its tip is suspended on a Ti macro-contact. The cap surface area is ~10^{-9} cm^2. b) Top: schematic of the chirality sensor. The Au-NF is suspended between two Ti contacts which are connected to a voltage source and an ammeter. The sensor is placed on an XYZ stage to allow alignment under the focused laser beam. The beam is focused by a microscope objective and passed through a quarter waveplate to generate circular polarization. The polarization is changed between left-circularly polarized light and right-circularly polarized light by a half waveplate positioned on a motorized stage. The sensor was monitored using a CCD camera.*

Because the shape and morphology of the NF gold cap is non-symmetric, it is not expected to be symmetric under a mirror reflection; hence, it possesses some degree of chirality. In addition, chiral metastructures can have strong optical activity[29,33] and even the LSPR of individual metallic nanoparticles can display some optical activity signal because of shape imperfections and crystal structure changes.[29] Thus, the Au-NF chirality sensor behaves differently under left and right circular polarizations prior to addition of a chiral analyte. To account for the non-zero signal response, the device is measured before and after exposure to the chiral analyte. Adsorption of the chiral analyte is confirmed by comparing the I-V curves, collected without illumination, before and after the exposure to the analyte. Note that the analyte adsorption changes the conductance gap of the junction, further indicating molecular adsorption; Figure S3 shows an example of a measurement in which an energy gap is formed.[34] This feature of the Au-NF device, acting as a nanogap device for electronic detection of molecules trapped at the Au-tip-Ti electrode gap was previously demonstrated (see references 34 and 35 for a more thorough analysis of this phenomenon). Further validation of the adsorption of a chiral analyte on the Au-NF was achieved by using CdSe quantum dots (QDs) as markers and confirmed using fluorescence microscopy (See Figure S1).

The effect of chiral molecule adsorption on the device at a 1V bias is demonstrated in Figure 2. Current-voltage (I-V) measurements showed gap formation following the introduction of an alpha-helix polyalanine (AHPA) solution, indicative of monolayer formation at the Au-cap-Ti electrode gap. Prior to introduction of chiral molecules, illumination of the device with 532 nm LCP (red) and RCP (blue) light generates an intrinsic chiral response from the device (Figure 2a). When the device structure is exposed to AHPA solution, an asymmetry in the polarized excitation is obtained and it depends on the handedness of the AHPA. Figure 2b shows the photoresponse after introducing AHPA-D molecules, where a change in photocurrent under different circular polarizations is observed, due to molecular adsorption. The relatively long stabilization times arise because the NF junctions were not passivated and thus surface states change upon molecular adsorption. Figure 2c shows that the difference in polarization dependent excitation (LCP – RCP) is positive for AHPA-D (red) and negative for AHPA-L (blue); see section 2 in the SI for a complete description of the calculation details. Control experiments using an achiral molecule, mercaptododecanoic acid (yellow), showed a negligible response. Studies using a mixture of both AHPA-D and AHPA-L enantiomers, with a small enantiomeric excess of AHPA-D (2.5 %), was also explored. Figure 2C shows that chiral response decreases, compared to the pure AHPA-D sample, and is in good agreement with CD measurements performed on the same solutions (see section 7 in the SI).

The measurement procedure was repeated with linearly polarized light illumination oriented parallel and perpendicular to the Au-NF's long axis. While a different photoresponse for the parallel and perpendicular illuminations is expected, a chiral molecule-dependent response is not expected since linear polarization is simply a superposition of left and right circular polarizations. Indeed, for both AHPA chiralities the same linear response is measured. (Figure 2d). In the linear

158 polarization measurement mode, both AHPA-L and AHPA-D showed a non-zero relative response
159 (see section 2 in the SI for a complete definition of the relative response), with the same sign and
160 magnitude for the two enantiomers. The specific chirality response is attributed to an induced
161 chirality effect[29] arising from adsorption of the chiral molecules at the NF gold nanocap.[41] Because
162 the device response using linear polarization relates to the density and coverage of adsorbed
163 molecules on the Au-NF, the absolute magnitude of the response can be used as a control. For
164 instance, a similar response for AHPA-D and AHPA-L under linear polarization indicates that the
165 different response obtained for the circular polarization is not associated with changes in the
166 molecular density at the Au-NF surface.

167 By varying the applied bias during photoexcitation, the photoconductance as a function of the
168 voltage applied across the junction was used to probe for molecules. The NF nanojunction device
169 is sensitive to the presence, and chirality, of molecules trapped between the gold nanocap and the
170 counter electrode.[34,42] The change in tunneling current upon formation of a molecular junction with
171 the analyte molecules can thus be used for recognition purposes, similar to previous reports.[42] It is
172 important to emphasize that the tunneling spectra are used here solely as an indicator for the
173 adsorption process. To demonstrate this concept, voltage sweeps between -2V to 2V were acquired
174 for three cases: no illumination, LCP illumination, and RCP illumination. The procedure was
175 repeated many times to account for long-term drift in the device. The conductance of the Au-NF
176 chirality sensor without illumination before and after exposure to AHPA-L solution is shown in
177 Figure S3. As described before, molecular adsorption resulted in the formation of an energy gap.
178 The gap is formed as a result of the tunneling spectroscopy of the molecules present between the
179 gold nanocap and the counter electrode. Figures 2e and 2f show the conductance measured under
180 LCP (red) and RCP (blue) illumination before and after exposure to AHPA-L, respectively. Only

minor differences in the conductance are observed before exposure to AHPA-L, however a distinct change is obtained when chiral molecules are introduced to the junction.

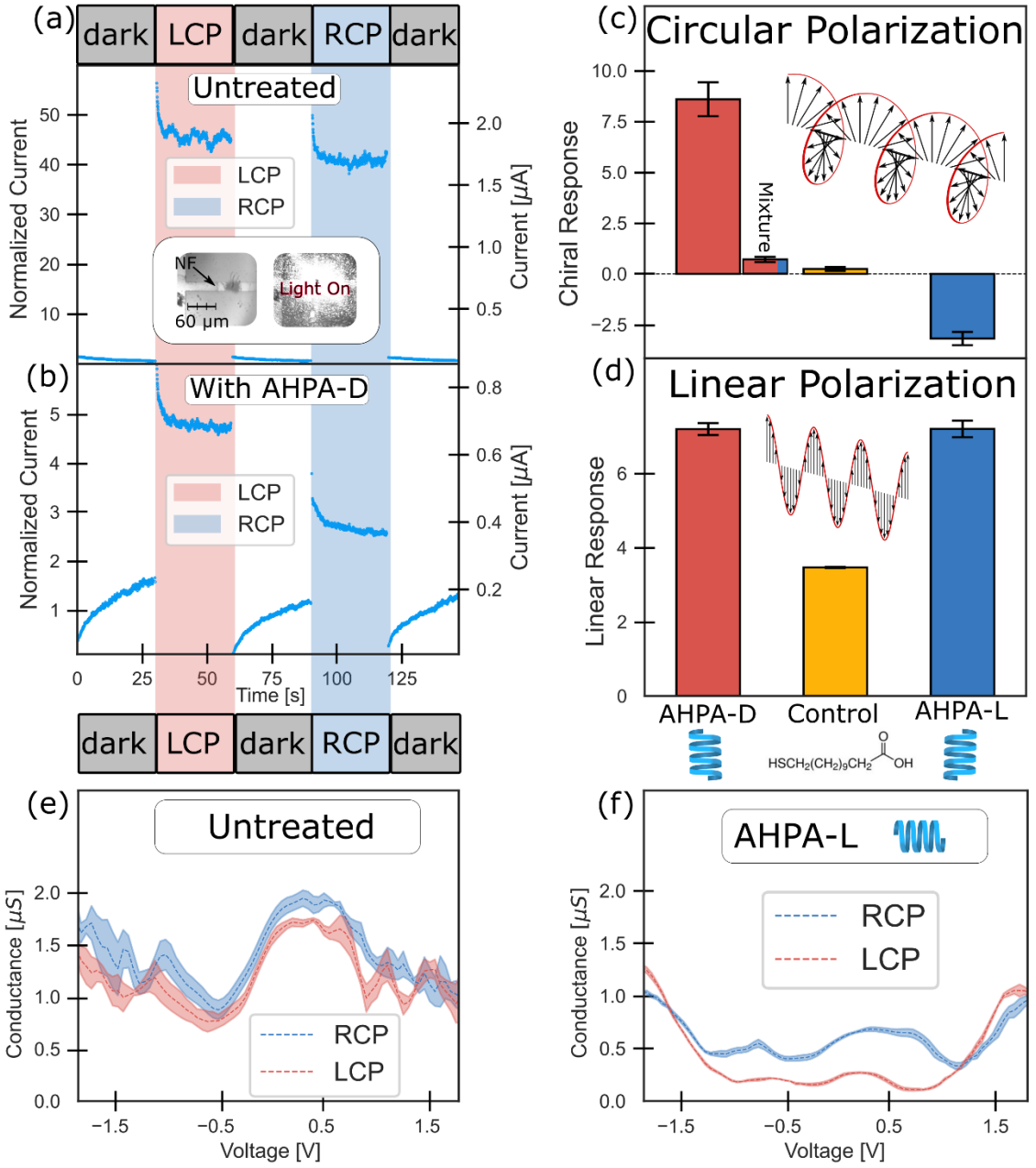

Figure 2. *Measurements of the Au-NF chirality sensor under a constant voltage. a) Current vs. time under a constant voltage of 1 Volt with different circular polarization illuminations and with no illumination, before molecules are dropcast. Inset: optical image of the Au-NF junction, with and without illumination. b) Current vs. time under a constant voltage with different circular*

polarization illuminations and with no illumination, after molecules are dropcast. c) The relative chiral response for the two enantiomers of AHPA and a control molecule, mercaptododecanoic acid, as well as a mixture with a 2.5 ee of AHPA-D d) Control experiment, measuring the response for parallel and perpendicular orientation of linear polarization. e) Numerical first derivative as a function of bias voltage before molecules are dropcast, showing a small difference between polarizations. f) Numerical first derivative as a function of bias voltage after molecules are dropcast, showing a clear difference between polarizations. The error in the dI/dV curves is the standard error of the mean at each point, marked as shaded area.

To explore possible contributions from plasmonic effects to the device response, the system was tested in the absence of chiral molecules in the conductance channel. Previous studies have shown that molecular desorption can be induced by applying a high voltage bias through the device.[42] Notably, considering the local electric field, desorption induced by applied voltage, is directed to molecules positioned at the molecular junction, leaving adsorbed molecules on the rest of NF gold cap. The adsorption and desorption are reflected by clear changes in the I-V curves in Figure 3c; where the change in shape of the current onset upon exposure to AHPA-L (yellow) is much more pronounced prior to desorption (red). See Figure S4 for real-time probing of the desorption process. Figure 3b shows that the tunneling current does not change significantly with an external magnetic field. Because gold becomes magnetic upon adsorption of thiolated chiral molecules,[53] and chiral molecules can act as spin filters due to the CISS effect,[52] one could expect differences in current with magnetization of the bottom gold contact. However, for this study the response is minimal. Figure 3d summarizes the magnitude of the chiral response before (blue) and after (red) molecular desorption. Interestingly, an increase in chiral response is observed. Because desorption of chiral molecules from the Au-NF should result in a slightly lower chiral induced LSPR, and hence decrease in chiral response, some contributions from spin selective transport through the molecule which act oppositely to chiral induced LSPR may be occurring. However, the primary mechanism which governs the chirality sensing is rooted in chiral induced LSPR. To demonstrate the universality of this technique, the chiral response of L-tryptophan was also measured. Unlike

AHPA, tryptophan is a smaller molecule and thus does not exhibit a chiral secondary structure. Consequently a smaller difference is seen in the *I(V)* curves after molecular adsorption (Figure 3e). As was the case for AHPA, the L-tryptophan response is larger for LCP than for RCP (Figure 3f). The calculated response is smaller than for polyalanine (-0.39 ± 0.02) as may be expected due to the shorter molecular length

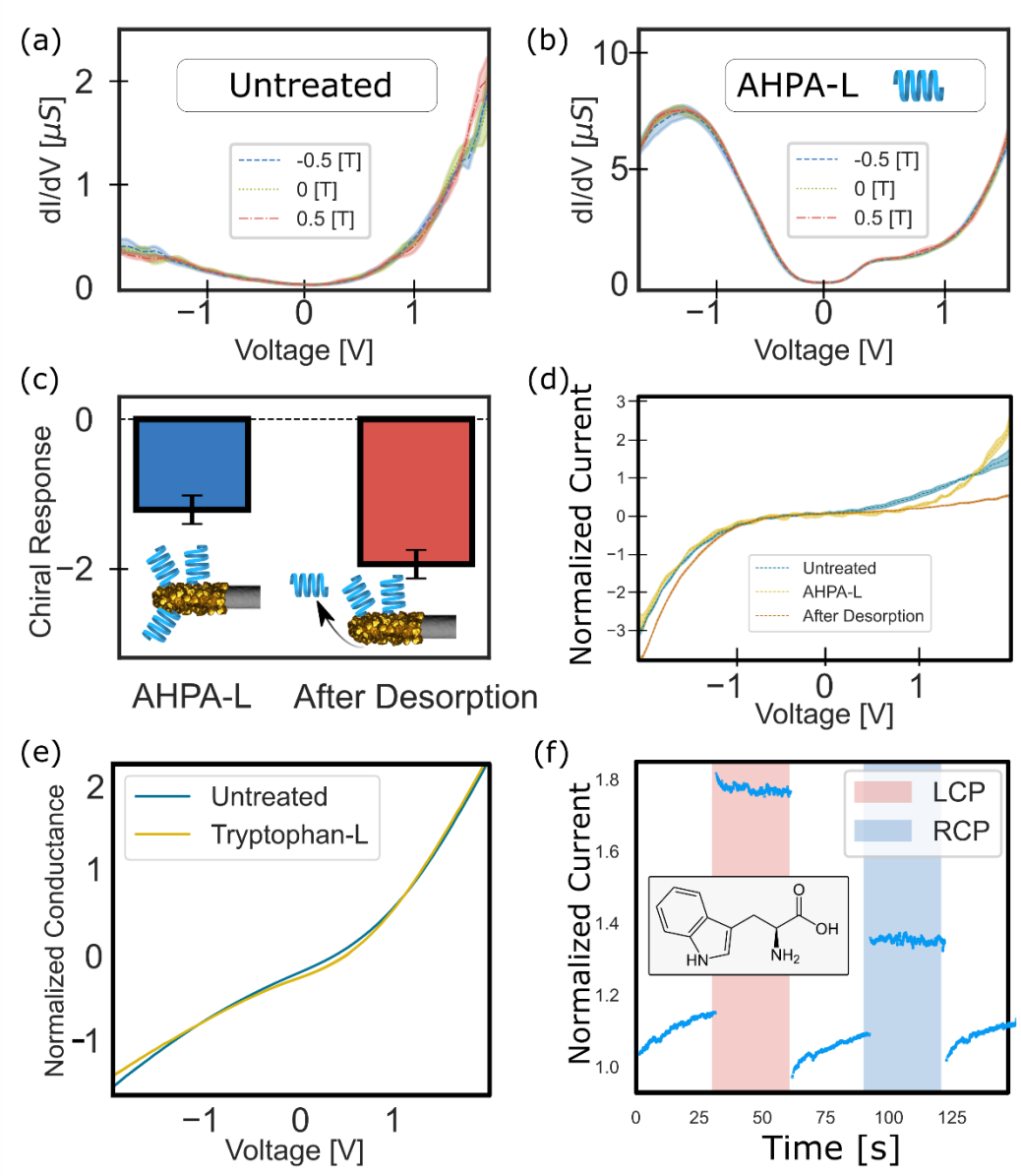

Figure 3. *a) dI/dV as a function of voltage under two opposite magnetic fields and zero magnetic field, showed negligible differences. b) The repeated experiment after AHPA-L is dropcast, show no differences between the applied magnetic fields. c) the chiral response before and after molecular desorption, showing that the chiral response remains d). I(V) curves at the three stages of the experiment, shown energy gap formation and disappearance of the energy gap after desorption. e) I(V) curves of L tryptophan before and after molecular adsorption. After adsorption a small gap is formed. f) the chiral response for tryptophan with LCP and RCP excitation. The response is large with LCP excitation.*

To further study the device functionality for detecting chiral species, CdSe quantum dots (QDs) capped with a chiral L-cysteine ligand were used to evaluate the effectiveness of the sensor towards analytes with an optical absorption wavelength that coincides with the polarized light wavelength. Figure S5 shows absorbance and CD spectra of the QDs capped with a chiral L-cysteine ligand which confirm it is optically active.[43–46] Figure 4a shows the chiral response (calculated as described in section 2 of the SI) of the sensor after it is exposed to the L-cysteine-CdSe QDs and illuminated with 532 nm (green) and 660 nm (red) light. The threshold for the onset of the QDs absorption is around 600 nm, therefore, light absorption by the QDs is negligible for illumination at wavelengths longer than 660 nm. A relatively small chiral response is obtained with 532 nm illumination and a negligible response is observed for 660 nm illumination - similar to the control experiments with achiral molecules. The wavelength dependent chiral response of the QDs suggests that the resonant coupling between the photoexcited QDs and the LSPR, similar to the mechanism of LSPR induced CD for chiral molecules,[31] plays a dominant role in the sensing mechanism. The chirality-dependent response for AHPA-L using the two illumination wavelengths is shown on the right side of Figure 4a for comparison. The broadband plasmonic

resonance of the NF gold cap extends to the short wave IR spectral range (SWIR),[36] in agreement with the observed chiral-sensitive response.

Illumination dependent conductance measurements for junctions with chiral QDs are shown in Figures 4b-d. When chiral QDs (yellow) are introduced to an untreated sensor (blue) a large change in the conductance is observed and is representative of the intrinsic bandgap of the QDs; see Figure 4b. The conductance measured using LCP (red) and RCP (blue) illumination show markedly different behavior when excited with 532 nm (Figure 4c) and 660 nm (Figure 4d) light. For 532 nm excitation the energy gap is reduced, whereas for 660 nm excitation the conductance appears similar in shape to the measurements made for the chiral QD in the dark. The different response for the QD system at wavelengths below and above the QDs energy gap indicate that coupling between the QD's excitation and the LSPR mode is the main mechanism responsible for the measured chiral response. That is the response at 660 nm is similar to that for AHPA-L, where no light adsorption of the analyte molecule is involved, and is attributed to chiral imprinting on the NF gold nanocap LSPR [cite reference 37: Goldsmith PCCP (2006)]. Interestingly, the chiral response of the AHPA-L molecules under 660 nm is opposite in sign to that found when using 532 nm light, and it is attributed to the bisignate shape of the optical activity,[47] similar to what has been shown for other coupled LSPR systems.[48–50]

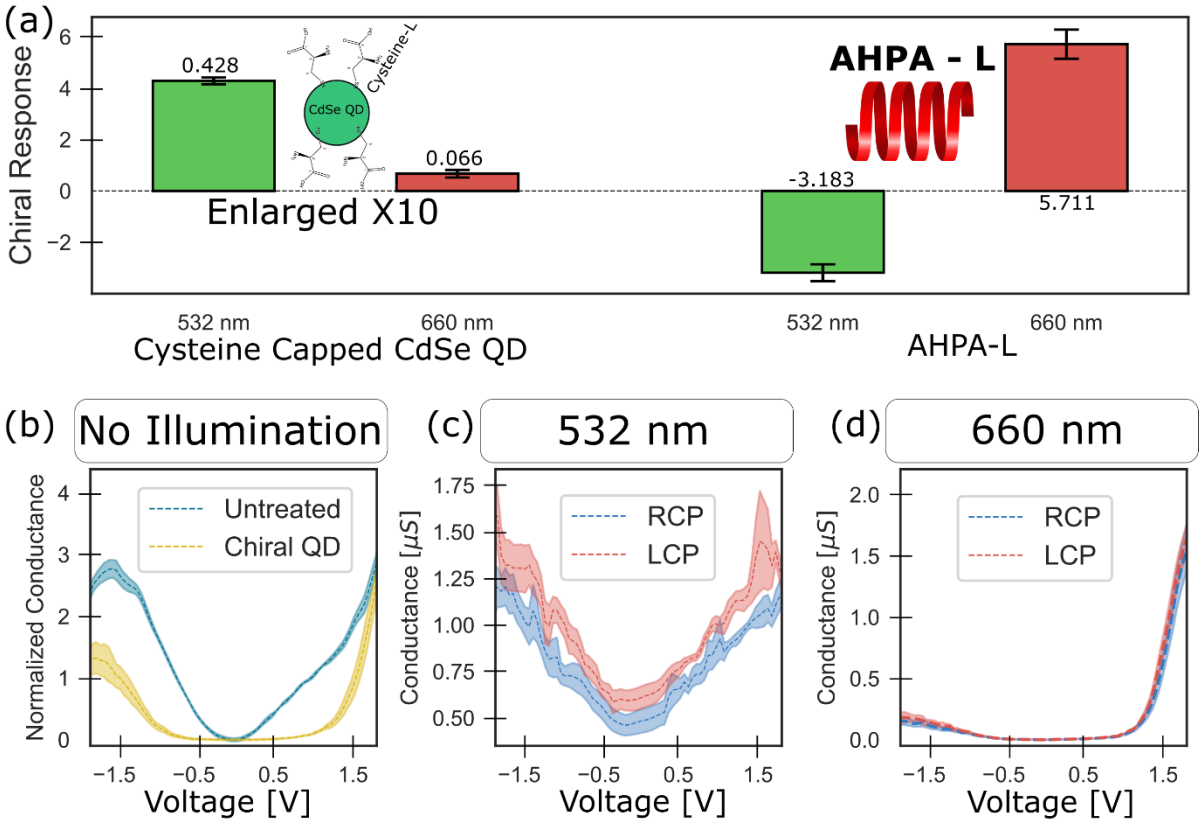

261

262 **Figure 4.** *Comparison between the chiral response of L-cysteine capped CdSe QDs and AHPA-L*
263 *molecules. a) A relatively small chiral response exists for QDs only under 532 nm illumination*
264 *while a chiral response occurs for both 532 nm and 660 nm illumination of AHPA-L. b) Z-score*
265 *normalized conductance vs. voltage curves before and after the dropcasting of L-cysteine capped*
266 *CdSe QDs without illumination. c) Conductance vs voltage curves of L-cysteine capped QDs*
267 *measured using 532nm LCP and RCP illumination. d) Conductance vs voltage curves of L-cysteine*
268 *capped QDs measured using 660nm LCP and RCP illuminations.*

269

270 Further control experiments were performed to assess the role of spin selective electron
271 transport. Previous studies have shown that charge transport through chiral media can be spin
272 selective[51] and has since been termed chiral induced spin selectivity (CISS).[52] Gold with chiral
273 molecules adsorbed on top may be magnetic,[53] and local magnetization can be imparted onto gold
274 nanoparticles by the gold-sulfur linkages.[54] To explore possible contributions from such
275 magnetization, Au-NF devices were studied without illumination under two opposite magnetic

fields and compared to zero magnetic field; (Figures 3a, b). The conductance measurements were invariant under the magnetic fields studied for pristine devices as well as after introduction of AHPA-L molecules, therefore, it is concluded that any effect of magnetization, if present, is negligible.

In summary, the present study demonstrates a novel chirality detection concept obtained by the coupling of a chiral plasmon response into an electrical current for detecting adsorbed chiral species, and its implementation in an electrical readout device. The chiral induced LSPR in the tunneling device is sensitive to the molecular chirality and provides information even for a small number of molecules adsorbed at the nano-gap junction. The device design eliminates the need of a chiral recognition element by sensing the chiral molecules' imprinting on the LSPR of the Au nanofloret and its coupling with electrical sensing. Experiments showing the change in chiral response with enantiomeric excess indicate the potential of the device for determining the enantiopurity of solutions, upon calibration. It is important to note that the device can also be used in a transient mode as was done in previous works[35] and can obviate the sensitivity to multilayer chiral organization.[55] Moreover, fabrication of the device is scalable and does not require advanced photolithography techniques or a complicated optical setup. The simplicity and generality of the chirality sensing method presented here, along with its real-time sensing capabilities, is advantageous for the sensing of enantiospecific materials, as well as for fundamental studies of chiral molecules at low concentrations and quantities. Relying on Au-NF hybrid nanostructures as the active sensing component, utilizing a bottom-up self-processing synthesis, and formation of self-adjusting nano-gap junctions enables a facile fabrication methodology that may be further utilized in the future to realize scalable and portable devices for real-time detection and chiral-specific analysis.

ASSOCIATED CONTENT

Supporting Information. Additional experimental information and calculation description can be found in the supporting information.

AUTHOR INFORMATION

Corresponding Author

*E-mail: roie.yerushalmi@mail.huji.ac.il

*E-mail: yossi.paltiel@mail.huji.ac.il

Funding Sources

D.H.W. acknowledges support from the United States National Science Foundation (CBET 1852588).

ACKNOWLEDGMENT

AZ would like to acknowledge the Israeli Ministry of Science, Technology and Space support.

REFERENCES

1. *Chirality in Natural and Applied Science*. Lough, W.J, Wainer I. W. (Blackwell, 2002).
2. Nguyen, L. A., He, H. & Pham-Huy, C. Chiral Drugs: An Overview. *Int J Biomed Sci* **2**, 85–100 (2006).
3. Machida, Y. & Nishi, H. Chiral Purity in Drug Analysis. in *Encyclopedia of Analytical Chemistry* (American Cancer Society, 2006). doi:10.1002/9780470027318.a1906.
4. Fanali, C., D'Orazio, G., Gentili, A. & Fanali, S. Analysis of Enantiomers in Products of Food Interest. *Molecules* **24**, (2019).

5. Garrison, A. W., Schmitt-Kopplin, P. & Avants, J. K. Analysis of the Enantiomers of Chiral Pesticides and Other Pollutants in Environmental Samples by Capillary Electrophoresis. in *Capillary Electrophoresis: Methods and Protocols* (ed. Schmitt-Kopplin, P.) 157–170 (Humana Press, 2008). doi:10.1007/978-1-59745-376-9_8.
6. Hierlemann, A., Baltes, H. & Schurig, V. Search for extraterrestrial enantioenrichment by using chemical microsensors. *Enantiomer* **6**, 129–139 (2001).
7. *Chiroptical Spectroscopy : Fundamentals and Applications*. (CRC Press, 2016). doi:10.1201/9781315374888.
8. Berova, N., Nakanishi, K. & Woody, R. W. *Circular Dichroism: Principles and Applications*. (John Wiley & Sons, 2000).
9. Grimme, S. D. A. Lightner and J. E. Hurst. Organic conformational analysis and stereochemistry from circular dichroism spectroscopy. Wiley-VCH, Weinheim, 2000. 487 pp. Price: US $ 99.95. ISBN 0-471-35 405-8. *Magnetic Resonance in Chemistry* **40**, 380–380 (2002).
10. Superchi, S., Giorgio, E. & Rosini, C. Structural determinations by circular dichroism spectra analysis using coupled oscillator methods: An update of the applications of the DeVoe polarizability model. *Chirality* **16**, 422–451 (2004).
11. Holzwarth, G., Hsu, E. C., Mosher, H. S., Faulkner, T. R. & Moscowitz, A. Infrared circular dichroism of carbon-hydrogen and carbon-deuterium stretching modes. Observations. *J. Am. Chem. Soc.* **96**, 251–252 (1974).
12. Mislow, K. Optical Rotatory Dispersion. Applications to Organic Chemistry. *J. Am. Chem. Soc.* **82**, 5769–5770 (1960).

13. Müller, T., Wiberg, K. B., Vaccaro, P. H., Cheeseman, J. R. & Frisch, M. J. Cavity ring-down polarimetry (CRDP): theoretical and experimental characterization. *J. Opt. Soc. Am. B, JOSAB* **19**, 125–141 (2002).
14. Bougas, L. *et al.* Chiral cavity ring down polarimetry: Chirality and magnetometry measurements using signal reversals. *J. Chem. Phys.* **143**, 104202 (2015).
15. Sofikitis, D. *et al.* Evanescent-wave and ambient chiral sensing by signal-reversing cavity ringdown polarimetry. *Nature* **514**, 76–79 (2014).
16. Schurig, V. Chiral shift reagents for NMR-spectroscopy. A simple and improved access to lanthanide-tris-chelates of d-3-TFA-camphor. *Tetrahedron Letters* **13**, 3297–3300 (1972).
17. Tsutsui, H. *et al.* Chiral amines as reagents for HPLC-MS enantioseparation of chiral carboxylic acids. *J Sep Sci* **35**, 1551–1559 (2012).
18. Zhu, G., Kingsford, O. J., Yi, Y. & Wong, K. Review—Recent Advances in Electrochemical Chiral Recognition. *J. Electrochem. Soc.* **166**, H205 (2019).
19. Trojanowicz, M. & Kaniewska, M. Electrochemical Chiral Sensors and Biosensors. *Electroanalysis* **21**, 229–238 (2009).
20. Ide, J., Nakamoto, T. & Moriizumi, T. Discrimination of aromatic optical isomers using quartz-resonator sensors. *Sensors and Actuators A: Physical* **49**, 73–78 (1995).
21. L, T. *et al.* A sensitivity-enhanced field-effect chiral sensor. *Nat Mater* **7**, 412–417 (2008).
22. Bodenhöfer, K. *et al.* Chiral Discrimination in the Gas Phase Using Different Transducers: Thickness Shear Mode Resonators and Reflectometric Interference Spectroscopy. *Anal. Chem.* **69**, 3058–3068 (1997).

23. Severin, E. J., Sanner, R. D., Doleman, B. J. & Lewis, N. S. Differential Detection of Enantiomeric Gaseous Analytes Using Carbon Black−Chiral Polymer Composite, Chemically Sensitive Resistors. *Anal. Chem.* **70**, 1440–1443 (1998).
24. Zhang, S., Ding, J., Liu, Y., Kong, J. & Hofstetter, O. Development of a Highly Enantioselective Capacitive Immunosensor for the Detection of α-Amino Acids. *Anal. Chem.* **78**, 7592–7596 (2006).
25. Shahgaldian, P., Hegner, M. & Pieles, U. A Cyclodextrin Self-Assembled Monolayer (SAM) Based Surface Plasmon Resonance (SPR) Sensor for Enantioselective Analysis of Thyroxine. *J Incl Phenom Macrocycl Chem* **53**, 35–39 (2005).
26. Ben-Amram, Y., Riskin, M. & Willner, I. Selective and enantioselective analysis of mono- and disaccharides using surface plasmon resonance spectroscopy and imprinted boronic acid-functionalized Au nanoparticle composites. *Analyst* **135**, 2952–2959 (2010).
27. Hofstetter, O., Hofstetter, H., Wilchek, M., Schurig, V. & Green, B. S. Chiral discrimination using an immunosensor. *Nature Biotechnology* **17**, 371–374 (1999).
28. Hazut, O. *et al.* Semiconductor–Metal Nanofloret Hybrid Structures by Self-Processing Synthesis. *J. Am. Chem. Soc.* **138**, 4079–4086 (2016).
29. Valev, V. K., Baumberg, J. J., Sibilia, C. & Verbiest, T. Chirality and Chiroptical Effects in Plasmonic Nanostructures: Fundamentals, Recent Progress, and Outlook. *Advanced Materials* **25**, 2517–2534 (2013).
30. Wang, X. & Tang, Z. Circular Dichroism Studies on Plasmonic Nanostructures. *Small* **13**, 1601115 (2017).

31. Lieberman, I., Shemer, G., Fried, T., Kosower, E. M. & Markovich, G. Plasmon-Resonance-Enhanced Absorption and Circular Dichroism. *Angewandte Chemie International Edition* **47**, 4855–4857 (2008).
32. A. Paiva-Marques, W., Reyes Gómez, F., N. Oliveira, O. & Mejía-Salazar, J. R. Chiral Plasmonics and Their Potential for Point-of-Care Biosensing Applications. *Sensors* **20**, 944 (2020).
33. W. Li, Z. J. Coppens, L. V. Besteiro, W. Wang, A. O. Govorov, J. Valentine. Circularly polarized light detection with hot electrons in chiral plasmonic metamaterials. *Nature Communications* **6**, 8379 (2015).
34. Ziv, A. *et al.* Self-formed nanogap junctions for electronic detection and characterization of molecules and quantum dots. *RSC Adv.* **7**, 25861–25866 (2017).
35. Karadan, P. *et al.* Molecular Fingerprint Detection Using Portable Water-Compatible Electronic Tunneling Spectroscopy Device. *Advanced Materials Interfaces* **n/a**, 2000605.
36. Ziv, A. *et al.* Broad-band high-gain room temperature photodetectors using semiconductor–metal nanofloret hybrids with wide plasmonic response. *Nanoscale* **11**, 6368–6376 (2019).
37. Goldsmith, M.-R. *et al.* The chiroptical signature of achiral metal clusters induced by dissymmetric adsorbates. *Phys. Chem. Chem. Phys.* **8**, 63–67 (2006).
38. Zhou, Y. *et al.* Flexible Linearly Polarized Photodetectors Based on All-Inorganic Perovskite CsPbI3 Nanowires. *Advanced Optical Materials* **6**, 1800679 (2018).
39. Bahlmann, K. & Hell, S. W. Depolarization by high aperture focusing. *Appl. Phys. Lett.* **77**, 612–614 (2000).
40. Lekner, J. Polarization of tightly focused laser beams. *J. Opt. A: Pure Appl. Opt.* **5**, 6–14 (2002).

41. Bezen, L. *et al.* Chiral Molecule-Enhanced Extinction Ratios of Quantum Dots Coupled to Random Plasmonic Structures. *Langmuir* **34**, 3076–3081 (2018).
42. Karadan, P. *et al.* Molecular Fingerprint Detection Using Portable Water-Compatible Electronic Tunneling Spectroscopy Device. *Advanced Materials Interfaces* **n/a**, 2000605.
43. Bloom, B. P., Graff, B. M., Ghosh, S., Beratan, D. N. & Waldeck, D. H. Chirality Control of Electron Transfer in Quantum Dot Assemblies. *J. Am. Chem. Soc.* **139**, 9038–9043 (2017).
44. Ben-Moshe, A., Teitelboim, A., Oron, D. & Markovich, G. Probing the Interaction of Quantum Dots with Chiral Capping Molecules Using Circular Dichroism Spectroscopy. *Nano Lett.* **16**, 7467–7473 (2016).
45. Tohgha, U., Varga, K. & Balaz, M. Achiral CdSe quantum dots exhibit optical activity in the visible region upon post-synthetic ligand exchange with D- or L-cysteine. *Chem. Commun.* **49**, 1844–1846 (2013).
46. Al-Bustami, H. *et al.* Optical Multilevel Spin Bit Device Using Chiral Quantum Dots. *Nano Lett.* **20**, 8675–8681 (2020).
47. Stephens, P. J. & Harada, N. ECD cotton effect approximated by the Gaussian curve and other methods. *Chirality* **22**, 229–233 (2010).
48. Guerrero-Martínez, A. *et al.* Intense Optical Activity from Three-Dimensional Chiral Ordering of Plasmonic Nanoantennas. *Angewandte Chemie International Edition* **50**, 5499–5503 (2011).
49. Auguié, B., Alonso-Gómez, J. L., Guerrero-Martínez, A. & Liz-Marzán, L. M. Fingers Crossed: Optical Activity of a Chiral Dimer of Plasmonic Nanorods. *J. Phys. Chem. Lett.* **2**, 846–851 (2011).

50. Fan, Z. & Govorov, A. O. Plasmonic Circular Dichroism of Chiral Metal Nanoparticle Assemblies. *Nano Lett.* **10**, 2580–2587 (2010).
51. Wei, J. J. *et al.* Molecular Chirality and Charge Transfer through Self-Assembled Scaffold Monolayers. *J. Phys. Chem. B* **110**, 1301–1308 (2006).
52. Naaman, R., Paltiel, Y. & Waldeck, D. H. Chiral molecules and the electron spin. *Nat Rev Chem* **3**, 250–260 (2019).
53. Al-Bustami, H. *et al.* Single Nanoparticle Magnetic Spin Memristor. *Small* **14**, 1801249 (2018).
54. Crespo, P. *et al.* Permanent Magnetism, Magnetic Anisotropy, and Hysteresis of Thiol-Capped Gold Nanoparticles. *Phys. Rev. Lett.* **93**, 087204 (2004).
55. Ha, N. T. N. *et al.* Charge-Ordered α-Helical Polypeptide Monolayers on Au(111). *J. Phys. Chem. C* **124**, 5734–5739 (2020).